Power-Efficient Hybrid MIMO Receiver with Task-Specific Beamforming using Low-Resolution ADCs

Timur Zirtiloglu, Nir Shlezinger, Yonina C. Eldar, and Rabia Tugce Yazicigil

Abstract—Multiple-input multiple-output (MIMO) systems utilize multiple antennas and signal acquisition chains, facilitating multi-user communications with increased spectral efficiency and better coverage via beamforming. MIMO systems are typically costly to implement and consume high power. A commonly used method to reduce the cost of MIMO receivers is to design hybrid analog/digital beamforming (HBF), which reduces the number of RF chains. However, the added analog circuitry involves active components whose consumed power may surpass that saved in RF chain reduction. An additional method to realize power-efficient MIMO systems is to use low-resolution analog-to-digital converters (ADCs), however, compromising signal recovery accuracy. In this work, we propose a power-efficient hybrid MIMO receiver with dedicated beamforming to mitigate spatial interferers in congested environments, utilizing low-quantization rate ADCs, jointly optimizing the analog and digital processing using task-specific quantization techniques. We present an efficient analog pre-processing hardware architecture utilizing sparse low-resolution vector modulators to reduce analog processing power while maintaining recovery accuracy. Supported by numerical simulations and power analysis, our power-efficient MIMO receiver achieves comparable signal recovery performance to power-hungry fully-digital MIMO receivers using high-resolution ADCs. Furthermore, our receiver outperforms the task-agnostic HBF receivers with low-quantization rate ADCs in recovery accuracy at lower power.

Index Terms— Analog-to-digital conversion, beamforming, hybrid architecture, MIMO, quantization.

I. INTRODUCTION

Widespread utilization of multiple-input multiple-output (MIMO) communications brings superior data capacity, improved coverage, and highly robust multi-user support [1]–[4]. While the theoretical gains of MIMO communications have been extensively studied, hardware implementations usually face practical trade-offs between power consumption, spectral efficiency, and fidelity [5]–[8]. MIMO receivers typically consist of multiple signal acquisition chains for spatial signal processing. Each signal acquisition chain consists of a radio-frequency (RF) front end performing RF signal amplification with low noise and then downconverting this RF signal to low baseband frequencies. This continuous-time analog signal in the baseband is translated to the digital domain for further processing. Analog-to-digital conversion is performed in two steps: the continuous-time analog signal is sampled and converted to a discrete-time signal and then quantized into a discrete-amplitude representation stored as digital bits [9]. This process is usually carried out in hardware using uniform scalar analog-to-digital converters (ADCs) [10]. MIMO systems traditionally apply brute-force data acquisition with spatial signal processing using high-resolution quantization and Nyquist sampling rates leading to high power consumption and hardware design complexity, especially in massive MIMO.

A common approach to mitigate the increased cost of MIMO receivers is to utilize fewer RF chains and ADCs than antenna elements via hybrid analog/digital beamforming (HBF). Such architectures incorporate an additional analog combiner circuit before the quantization, allowing dimensionality reduction [11], [12] while preserving the ability

of the MIMO array in achieving directed beamforming via, e.g., holographic techniques [13]. In fact, HBF is also utilized without RF chain reduction to boost pre-acquisition spatial interferer rejection [14]–[17]. Nonetheless, the introduction of an analog combiner comprised of active components may also be power-hungry. An additional power reduction technique is to use low-resolution acquisition, connecting each antenna to a low-quantization rate ADC [18]–[21]. However, the distortion added by coarse quantization results in degraded signal recovery.

Recently, a task-specific (task-based) quantization framework was introduced to design MIMO receivers utilizing bit-constrained ADCs [22]–[25] while achieving accurate signal recovery. For task-specific quantization, the analog pre-processing front end is designed to be aware of the use of low-resolution ADCs and the desired task. Task-specific receivers combine the signals in the analog domain such that the quantization distortion hardly affects the low-dimensional task information recovered in digital. The task-specific approach achieves improved signal recovery in MIMO communications [8], [26], [27], and radar [28]. Despite its numerically evaluated performance gains, implementing MIMO receivers utilizing task-specific quantization requires an analog pre-processing front end, i.e., analog combiner, which may be costly and power-hungry. Therefore, it is essential to develop a power-efficient design methodology for the task-specific MIMO systems.

In this work, we study power-efficient hybrid MIMO receivers implementing bit-constrained signal recovery. We focus on MIMO communications in congested environments, where multiple users may be operating simultaneously, creating undesired interference. Hence, our task is to achieve simultaneous recovery of the desired signals and rejection of the interferers. Since power consumption is highly implementation-dependent, in this paper, we consider analog combiners implemented using vector modulators (VMs) [29]. We exploit boosting the VMs to be either discrete or sparsely activated since the power consumption is directly proportional to utilized hardware complexity [11], [30]. We propose a task-specific algorithm co-integrating these hardware-level techniques to achieve an accurate and power-efficient recovery of the desired task information. We present a hardware architecture utilizing low-resolution ADCs and a programmable analog pre-processing front end. By developing a model for end-to-end system evaluation, we compare the proposed system performance against task-agnostic MIMO systems in terms of signal recovery accuracy and receiver beam pattern via numerical simulations. Next, we provide power consumption estimates for the proposed and benchmark systems derived from the measured power consumption of the state-of-the-art (SOA) hardware implementations. At a significantly reduced quantization rate, we show that our design achieves accurate signal recovery comparable to the performance of the fully-digital MIMO receivers using high-resolution ADCs. Furthermore, the task-specific receiver notably outperforms such task-agnostic architectures operating under similar bit constraints. Regarding beam pattern, we demonstrate that our design attenuates the interferers by $\geq$ 36dB. Finally, the task-specific receiver reduces the power consumption by at least 58% compared to task-agnostic fully-digital MIMO and HBF receivers.

The rest of the paper is organized as follows: Section II reviews the system model. The HBF design algorithm is provided in Section III. Section IV presents the receiver architecture and our model-based performance evaluation supported with numerical simulations and power consumption estimates, and Section V concludes the paper.

T. Zirtiloglu and R. T. Yazicigil are with the ECE Department, Boston University, MA (e-mail:{timurz, rty}@bu.edu). N. Shlezinger is with the School of ECE, Ben-Gurion University of the Negev, Beer-Sheva, Israel (e-mail: nirshl@bgu.ac.il). Y. C. Eldar is with the Faculty of Math and CS, Weizmann Institute of Science, Rehovot, Israel (e-mail: yonina.eldar@weizmann.ac.il).
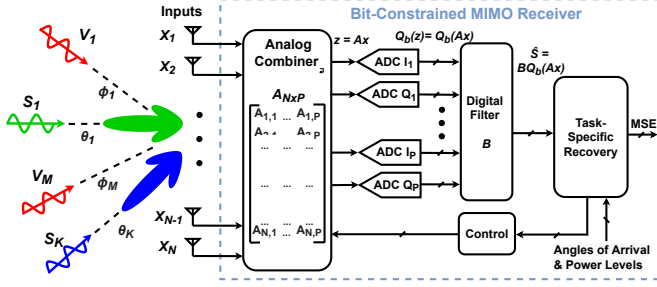
Fig. 1: Task-Specific hybrid MIMO receiver system with embedded beamforming and low-quantization rate ADCs.

II. SYSTEM MODEL

A. Task-Specific Hybrid MIMO with Embedded Beamforming

Consider a hybrid MIMO receiver with N antenna elements and P RF chains and ADCs. Let $\boldsymbol{x} = [x_1, \ldots, x_N]^T$ be signal observed at the N elements. The received signal is first processed in analog, yielding the vector $\boldsymbol{z} = [z_1, \ldots, z_P]^T$, which is forwarded to the ADCs. Let $\boldsymbol{A}$ be the $P \times N$ analog pre-processing matrix, the output vector $\boldsymbol{z}$ is

$$\boldsymbol{z} = \boldsymbol{A}\boldsymbol{x}. \tag{1}$$

The vector $\boldsymbol{z}$ is converted to a digital representation using P identical uniform ADCs, each with b levels, i.e., the overall number of bits used is $P\lceil \log_2 b \rceil$. The resulting vector processed in digital is $\mathcal{Q}_b(\boldsymbol{z})$, where $\mathcal{Q}_b(\cdot)$ is the element-wise uniform quantization operator with b levels.

The received vector $\boldsymbol{x}$ incorporates a set of K desired signals, denoted by $s_1, \ldots, s_K$, received from sources at relative angles $\theta_1, \ldots, \theta_K$, respectively. In addition, the received vector also includes M interferer components $v_1, \ldots, v_M$ received from sources at relative angles $\phi_1, \ldots, \phi_M$, respectively. All sources are assumed to be narrowband and lying at the far-field, and thus the noisy received signal is given by

$$\boldsymbol{x} = \sum_{k=1}^{K} s_k \boldsymbol{a}(\theta_k) + \sum_{m=1}^{M} v_m \boldsymbol{a}(\phi_m) + \boldsymbol{w}. \tag{2}$$

In (2), $\boldsymbol{w}$ is additive white Gaussian noise with variance σ_w^2, and $\boldsymbol{a}(\theta)$ is the $N \times 1$ steering weights vector whose entries are given by

$$[\boldsymbol{a}(\theta)]_n = e^{-j2\pi n \frac{d}{\lambda}\sin(\theta)}, \tag{3}$$

where d is the element spacing and λ is the wavelength. An illustration of this system is depicted in Fig. 1.

By defining the steering matrices $\boldsymbol{A}_\theta \in \mathcal{C}^{N \times K}$ and $\boldsymbol{A}_\phi \in \mathcal{C}^{N \times M}$ such that $[\boldsymbol{A}_\theta]_{n,k} = [\boldsymbol{a}(\theta_k)]_n$ and $[\boldsymbol{A}_\phi]_{n,m} = [\boldsymbol{a}(\phi_m)]_n$, as well as $\boldsymbol{s} = [s_1, \ldots, s_K]^T$ and $\boldsymbol{v} = [v_1, \ldots, v_M]^T$, we can write (2) as

$$\boldsymbol{x} = \boldsymbol{A}_\theta \boldsymbol{s} + \boldsymbol{A}_\phi \boldsymbol{v} + \boldsymbol{w}. \tag{4}$$

Based on (4), the second-order statistical moments of the observed $\boldsymbol{x}$ is $\boldsymbol{C_x} = \boldsymbol{A}_\theta \boldsymbol{C_s} \boldsymbol{A}_\theta^H + \boldsymbol{A}_\phi \boldsymbol{C_v} \boldsymbol{A}_\phi^H + \sigma_w^2 \boldsymbol{I}_N$, while its correlation with the task of interest $\boldsymbol{s}$ is given by $\boldsymbol{C_{sx}} = \boldsymbol{C_s} \boldsymbol{A}_\theta^H$. Here, $\boldsymbol{C_s}$ and $\boldsymbol{C_v}$ denote the covariance matrices of $\boldsymbol{s}$ and $\boldsymbol{v}$, respectively. These statistical measures are utilized for the task-specific recovery problem.

B. Problem Formulation

Our goal is to tune the analog combiner $\boldsymbol{A}$ of the HBF MIMO receiver based on the signal model in (4). Our design is optimized for multiple tasks, including (1) accurate signal recovery, (2) spatial interferer suppression, and (3) power efficiency.

Signal Recovery: The main task of the receiver is to recover the desired signal $\boldsymbol{s}$ from the digital representation $\mathcal{Q}_b(\boldsymbol{z})$. Our design

measure here is the mean-squared error (MSE), a common design objective for signal recovery. The MSE is defined by

$$\mathrm{MSE}(\boldsymbol{A}) := \mathbb{E}\left\{ \| \boldsymbol{s} - \mathbb{E}\{\boldsymbol{s}|\mathcal{Q}_b(\boldsymbol{A}\boldsymbol{x})\} \|^2 \right\}. \tag{5}$$

Interferer Suppression: The MSE objective focuses only on the ability to recover $\boldsymbol{s}$. As such, it may prefer settings of $\boldsymbol{A}$ in which the effect of $\boldsymbol{v}$ is mitigated via digital processing. In practice, it is often preferable to reject interferers in the analog domain. The strong spatial interferers may lead to receiver desensitization and increased dynamic range requirement of ADCs [16]. Consequently, we also explicitly require the analog combiner to suppress the spatial interferers. Since the contribution of $\boldsymbol{v}$ on the analog combiner output $\boldsymbol{z}$ takes the form $\boldsymbol{A}\boldsymbol{A}_\phi$, we penalize interferer rejection via the max norm of $\boldsymbol{A}\boldsymbol{A}_\phi$, i.e.,

$$\mathrm{IntRej}(\boldsymbol{A}) := \|\boldsymbol{A}\boldsymbol{A}_\phi\|_{\max} = \max_{i,j}\left(|[\boldsymbol{A}\boldsymbol{A}_\phi]_{i,j}|\right). \tag{6}$$

Power Efficiency: The power consumption of MIMO receiver front end is dictated by the individual cost of each hardware component, including local oscillators generation (LO Gen), RF amplifiers, mixers, filters, and ADCs. The use of low-resolution quantizers notably reduces the ADC power consumption, which is approximately proportional to the number of levels b [10]. In this work, we consider the design of the analog combiner $\boldsymbol{A}$ implemented using VMs. When using VMs, the elements of $\boldsymbol{A}$ cannot take any value in $\mathcal{C}$, and are constrained to some discrete set $\mathcal{A} \subset \mathcal{C}$, including $0 \in \mathcal{A}$, i.e. when VM is deactivated. In this case, the power consumption of an analog combiner $\boldsymbol{A}$ is highly dependent on two factors: how many different values can its entries take, i.e., $|\mathcal{A}|$, and which of its entries are active, namely, the sparsity level of $\boldsymbol{A}$. If the sparsity level of $\boldsymbol{A}$ increases while reducing its resolution, i.e., using a coarse $\mathcal{A}$, the power consumption of the receiver significantly reduces.

III. TASK-SPECIFIC LOW-POWER ACQUISITION

Here, we introduce an end-to-end design algorithm for the HBF MIMO receiver. We consider the case where the number of ADCs, their resolution b, and mapping of the VMs $\mathcal{A}$ are dictated by the hardware, and optimize $\boldsymbol{A}$ accordingly. We focus on signal recovery in Section III-A, then we incorporate interferer suppression and power reduction in Section III-B. We summarize the design in Section III-C.

A. Signal Recovery via Task-Specific Quantization

Recovering $\boldsymbol{A}$ which minimizes (5) is a special case of the task-specific (task-based) quantization setup studied in [22]. There, it was shown that while minimizing (5) is likely to be analytically intractable, one can obtain accurate signal recovery by modeling the ADCs as implementing non-subtractive dithered quantization, while aiming to recover the linear minimal MSE estimate of $\boldsymbol{s}$, i.e., the digital processing outputs an estimate of the form $\hat{\boldsymbol{s}} = \boldsymbol{B}\mathcal{Q}_b(\boldsymbol{A}\boldsymbol{x})$ for some $\boldsymbol{B} \in \mathcal{C}^{K \times P}$.

To formulate the MSE objective under the above considerations, define $\boldsymbol{\Gamma} \triangleq \boldsymbol{C_{sx}}\boldsymbol{C_x}^{-1/2}$, and let $\{\lambda_{\boldsymbol{\Gamma},i}\}$ be its singular values arranged in descending order. Also, set $\kappa \triangleq \eta^2\left(1 - \frac{\eta^2}{3b^2}\right)^{-1}$, where η is a coefficient tuned to guarantee negligible overloading probability of the ADCs (set here to $\eta = 3$). We can now reformulate the MSE in (5) as stated in the following lemma (adapting [22, Lem. 1] to complex signals):

Lemma 1. *When the ADCs utilize non-subtractive dithered quantizers with vanishing overloading probability, the MSE objective* (5) *becomes*

$$\mathrm{MSE}(\boldsymbol{A}) = \mathrm{Tr}\left(\boldsymbol{\Gamma}\boldsymbol{C_x}\boldsymbol{\Gamma}^H - \boldsymbol{\Gamma}\boldsymbol{C_x}\boldsymbol{A}^H\left(\boldsymbol{A}\boldsymbol{C_x}\boldsymbol{A}^H \right.\right.$$
$$\left.\left. + \frac{2\kappa \cdot \mathrm{Tr}(\boldsymbol{A}\boldsymbol{C_x}\boldsymbol{A}^H)}{3b^2 \cdot P}\boldsymbol{I}_P \right)^{-1}\boldsymbol{A}\boldsymbol{C_x}\boldsymbol{\Gamma}^H \right). \tag{7}$$

This MSE is achieved by setting the digital filter to be

$$B(A) = \Gamma C_x A^H \left(A C_x A^H + \frac{2\kappa \cdot \mathrm{Tr}(A C_x A^H)}{3b^2 \cdot P} I_P \right)^{-1}. \quad (8)$$

While Lemma 1 rigorously holds under some limiting assumptions on the system operation, i.e., using non-subtractive dithered quantizers, it also approximately holds when these assumptions are not satisfied for a broad range of input signals [22]. Furthermore, as shown in [22], the MSE objective in (7) is convex. In the following, we exploit this convexity to incorporate additional design considerations such that A is optimized while meeting the requirements detailed in Section II-B.

B. Low-Power Interferer Suppression

The objective (7) admits a closed-form minimizer, see [22, Thm. 1]. However, such a design only considers the signal recovery task and does not impose any structure on A. To account for the interference rejection requirement and to balance the power consumption of the analog circuitry, we formulate our design objective as

$$\mathcal{L}(A) = \mathrm{MSE}(A) + \gamma_I \mathrm{IntRej}(A) + \gamma_S \|A\|_{1,1}. \quad (9)$$

In (9), $\|\cdot\|_{1,1}$ is the entry-wise ℓ_1 norm operator, while $\gamma_I, \gamma_S \geq 0$ are regularization coefficients, balancing the contribution of signal recovery MSE, spatial interferer rejection, and sparsity level of analog combiner in the overall loss measure $\mathcal{L}(A)$. The interferer rejection regularization term defined in (6) is convex [31, Ch. 3.2], while sparsity of A is boosted in a manner that preserves convexity by adding the entry-wise ℓ_1 norm.

The final consideration which is not accounted for in (9) is the usage of discretized VMs. The resulting optimization is thus formulated as

$$A^\circ = \underset{A \in \mathcal{A}^{P \times N}}{\arg\min} \mathcal{L}(A). \quad (10)$$

The fact that the optimization problem (5) is formulated over a discrete (i.e., non-convex) search space makes obtaining the analog combiner that optimizes the objective within the constrained set extremely challenging. Nonetheless, as the objective $\mathcal{L}(A)$ is convex, one can utilize discrete optimization to recover suitable designs of A, as we do next.

C. Analog Combiner Design

Design Algorithm: Since the optimization problem (10) seeks to minimize a convex objective over a discrete set, we tackle it using projected convex optimization. Our design strategy is comprised of $k_{\max}$ rounds of a convex optimizer for minimizing $\mathcal{L}(A)$ over $\mathcal{C}^{P \times N}$, with periodic projections onto the discrete $\mathcal{A}$. We use $\mathcal{O}_\mathcal{L}(\cdot)$ to denote the iterative optimizer with loss measure $\mathcal{L}$. By using proximal gradient descent with step-size $\mu > 0$ while treating $\tilde{\mathcal{L}}(A) := \mathrm{MSE}(A) + \gamma_I \mathrm{IntRej}(A)$ as the task term and $\|A\|_{1,1}$ as the prior, thus guaranteeing sparsity of the analog combiner, it holds that [32, Ch. 3]

$$\mathcal{O}_\mathcal{L}(A) = \arg \min_{\tilde{A} \in \mathcal{C}^{P \times N}} \gamma_S \|\tilde{A}\|_{1,1} + \frac{1}{2} \left\| \tilde{A} - A + \mu \nabla_A \tilde{\mathcal{L}}(A) \right\|_{2,2}^2$$
$$= \mathcal{T}_{\gamma_S} \left\{ A - \mu \nabla_A \left(\mathrm{MSE}(A) + \gamma_I \mathrm{IntRej}(A) \right) \right\}. \quad (11)$$

Here, $\mathcal{T}$ is the element-wise complex soft-thresholding operator, given by $\mathcal{T}_\lambda(z) := e^{j \arg(z)} \max(|z| - \lambda, 0)$. Every k_{proj} iterations, the intermediate $A^{(k)}$ is projected to account for the discrete VMs via the element-wise projection operator $\mathcal{P}_\mathcal{A}(z) := \arg\min_{a \in \mathcal{A}} \|a - z\|_2$. The resulting algorithm is summarized as Algorithm 1.

The main hyperparameters of Algorithm 1 are the regularization coefficients γ_I, γ_S, the iteration limits $k_{\max}, k_{\mathrm{proj}}$, and the initial setting of $A^{(0)}$. These add up to the individual hyperparameters of the convex optimizer $\mathcal{O}_\mathcal{L}(\cdot)$. In our experimental study, where the number of complex ADCs is equal to the number of desired sources, i.e., $P = K$, we use $A^{(0)} = \Gamma$ as our initial estimate and set the digital filter via (8).

Discussion: Algorithm 1 allows tuning of the HBF receivers to accurately carry out signal recovery and interferer rejection tasks while boosting low-power implementation. In Section IV, we show that by utilizing Algorithm 1 to design a task-specific HBF receiver with low-resolution ADCs and quantized VMs with sparsity, one can achieve

---

Algorithm 1: Analog combiner setting

Init: Fix $A^{(0)}$
1 **for** $k = 1, 2, \ldots, k_{\max}$ **do**
2   Update $A^{(k)} \leftarrow \mathcal{O}_\mathcal{L}(A^{(k-1)})$
3   **if** $\mod(k, k_{\mathrm{proj}}) = 0$ **then**
4   Project via $A^{(k)} \leftarrow \mathcal{P}_\mathcal{A}(A^{(k)})$
5   **end**
6 **end**
Output: Analog combiner $A^{(k_{\max})}$.

---

comparable or improved MSE compared to task-agnostic HBF receivers, while consuming half the power at a $4\times$ reduced quantization rate.

The proposed tuning of the analog combiner requires prior knowledge of the angle of arrivals and power levels. These are used to form the correlation matrices C_x and C_{sx} used by the algorithm. This information should therefore be either estimated or externally provided by a spatial sensor. Furthermore, one of the open challenges is to analyze the impact of hardware non-idealities on the task-specific MIMO system performance, such as frequency-independent and -dependent gain and phase imbalance of vector modulators. This future study will enable us to design a co-optimized solution between the hardware and algorithms to cope with these issues. Finally, in our simulations, we manually select the hyperparameters of Algorithm 1. However, the recent success of deep learning tools in enabling rapid optimization [33] indicate that one can design data-driven hyperparameter setting via, e.g., the learn-to-optimize framework [34] or via deep unfolding [35]. The latter was recently shown in [36] to be particularly suitable for realizing accurate and fast optimization of convex objectives over discrete sets as in (10). This extension of our design algorithm is left for future study.

IV. TASK-SPECIFIC HYBRID MIMO SYSTEM EVALUATION

In this section, we evaluate the proposed MIMO receiver system. in Section IV-A. Next, in Section IV-B, we characterize the signal recovery performance using the MSE metric. We demonstrate the robustness of the system to spatial interferers by showing angular-dependent beampatterns of the analog combiner front end model in Section IV-C. Finally, we provide power consumption estimates in Section IV-D.

A. Hardware Architecture and Model-Based Simulation Setup

We model a task-specific MIMO hardware system to evaluate performance improvements compared to task-agnostic MIMO receivers and estimate power savings from the proposed task-specific quantization techniques. Our hardware system features an RF analog-combiner front end and digital signal processing (DSP) back end for task-specific recovery similar to the system illustration shown in Fig. 1. The RF analog-combiner front end consists of reconfigurable VMs with low noise, each assigned to a value of a specific matrix A entry. For an $N \times P$ front end, a total of $N \times P$ VMs have to be utilized. The system is configured using the prior knowledge of the angle of arrivals and signal power, as mentioned in Section III-C. The coefficients of the analog-combiner matrix A are computed according to Algorithm 1 in the DSP back end, and the VMs are configured using a control module. The N-element input observations $x = [x_1, \ldots, x_N]^T$ are fed into the analog combiner at RF frequencies, downconverted to a low baseband frequency, and provided to the low-quantization rate ADCs as in- and quadrature-phase signals (I & Q). In the digital domain, the filter B, computed using (8), is applied and signal recovery is performed. Performance is characterized using MSE.

For our simulations, we consider an 8×2 hybrid MIMO system, with $K = 2$ desired signals at angles $\theta_1 = \frac{\pi}{8}, \theta_2 = -\frac{\pi}{4}$ with variances 1.5 and 0.5, respectively. Additionally, we model $M = 2$ unwanted interferers at angles $\phi_1 = -\frac{\pi}{18}, \phi_2 = \frac{\pi}{3}$ with variances 5 for both sources. Consequently, the interferers are several times stronger than
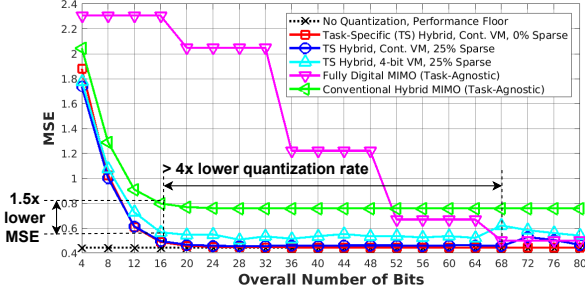
Fig. 2: MSE vs. total number of quantization bits for recovering $K = 2$ desired signals in the presence $M = 2$ spatial interferers.

(a) Array factor plot for output 1   (b) Array factor plot for output 2

Fig. 3: AF plots vs. angle of arrival for $P = 2$ outputs (dB scale, 20log).

the desired signals. The noise level is set to $\sigma_w^2 = 1$. For comparison purposes, we also evaluate the performance of the system without any quantization. In addition, we model a task-agnostic 8×2 conventional hybrid MIMO receiver with beamforming in analog and recovery in digital, and a task-agnostic 8×8 fully-digital MIMO receiver recovering the data solely in the digital domain, as benchmark systems.

B. MSE Performance

We evaluate the signal recovery MSE performance achieved using Algorithm 1 for various levels of analog pre-processing matrix $\boldsymbol{A}$ sparsity and VM resolution. The MSE in recovering $\boldsymbol{s}$ versus the overall number of bits, i.e., $P\lceil \log_2 b \rceil$, is depicted in Fig. 2. We show the numerical simulation results for sparsity levels of 0 and 25% with non-quantized, continuous (Cont.) matrix $\boldsymbol{A}$, and for 25% sparse $\boldsymbol{A}$ with VMs quantized with relatively low resolution, e.g., 4-bit resolution. We observe in Fig. 2 that by utilizing Algorithm 1, one can design a task-specific hybrid MIMO receiver using low-quantization rate ADCs to approach the MSE performance achieved without any quantization, while using low-resolution VMs, e.g., merely $2^4 = 16$ different settings for 4 bits, and deactivating 25% of VMs for sparsity to reduce power.

The task-agnostic fully-digital MIMO receiver achieves substantially worse MSE performance at a comparable total ADC bit budget. For the same targeted MSE performance floor, more than $4\times$ quantization rate reduction is observed with the proposed method. The conventional hybrid MIMO receiver, which only beamforms towards the desired angles and does not account for the interferers, also demonstrates worse recovery performance. Thus, the proposed method shows $1.5\times$ lower MSE at the same quantization rate of 16 bits, as shown in Fig. 2.

C. Task-Specific Beamforming and Array Factors

Algorithm 1 designs the analog combiner to reject the spatial interferers in analog, jointly optimized with the main system task of recovering the desired signals, $\boldsymbol{s}$, in digital. We model and compute the array factor (AF), illustrating the suppression of interferers in the spatial domain. The array factor is a measure of MIMO receiver gain as a function of an incoming signal's angular direction and defined as $AF(\theta) = \sum_{i=1}^{N} A_i e^{j\pi i \sin(\theta)}$, where A_i is a specific complex gain coefficient applied to the input signal, and N is the number of input antennas [14]. For an $N \times P$ MIMO receiver, there would be P independent beams directed towards a specific angle.

The AF computed at the $P = 2$ analog outputs of the proposed system is illustrated in Fig. 3, and is compared with a task-agnostic conventional hybrid MIMO receiver whose analog combiner beamforms towards θ_1 (Fig. 3a) and θ_2 (Fig. 3b). The beam patterns achieved by Algorithm 1 are directed towards both the desired angles θ_1 and θ_2, forming a linear combination of the desired signals at the output, while suppressing the interferers at angles ϕ_1, ϕ_2 by ≥ 36dB. However, as observed in Fig. 3, since the analog combiner is not only optimized for beamforming but rather designed for facilitating recovery from quantized observations, our analog combiner achieves lower AF gain for the desired signals compared to the conventional beamforming. Nonetheless, the lower AF gain does not harm the task-specific recovery accuracy (Fig. 2).
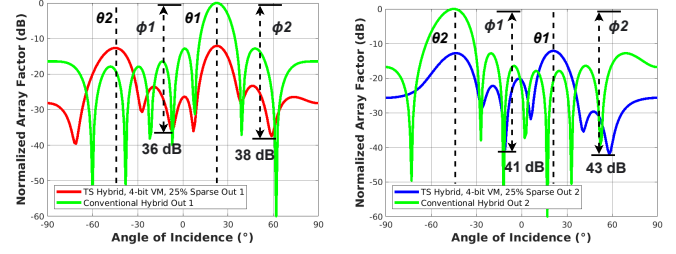
Hardware Component / System	Power (mW)
LNA/VM $P_{\mathrm{LNA/VM}}$ (1-5 GHz 8 bit/4 bit) [15], [37]	20/10
Mixer with LO Gen (1-5 GHz) P_{MIX} [38], [39]	15
Baseband Amplifier P_{BB} [11]	5
ADC P_{ADC} (100 MS/s 10 bit/4 bit) [40], [43]	10/0.5
Fully-Digital MIMO Receiver (8×8)	520
Conventional Hybrid MIMO Receiver (8×2)	410
Task-Specific Hybrid MIMO Receiver (8×2)	**172**

TABLE I: Estimated power consumption comparison.

D. Power Consumption Model

We estimate the power consumption of the proposed task-specific HBF MIMO receiver and the task-agnostic benchmark systems by using the measured power consumption of individual hardware components reported in the SOA integrated designs [11], [15], [37]–[41]. Power consumption of an $N \times N$ fully-digital MIMO receiver is estimated by:

$$P_{\mathrm{FD}} = N \cdot P_{\mathrm{LNA}} + N \cdot P_{\mathrm{MIX}} + 2 \cdot N \cdot P_{\mathrm{BB}} + 2 \cdot N \cdot P_{\mathrm{ADC}}. \quad (12)$$

Here, P_{LNA} is the power consumed by a low-noise amplifier, P_{MIX} is the power of the mixer, and P_{BB} and P_{ADC} are baseband amplifier and ADC power consumption, respectively, doubled for I & Q paths. The power consumed by an $N \times P$ hybrid MIMO receiver is estimated by:

$$P_{\mathrm{HYB}} = \gamma_{SP} \cdot N \cdot P \cdot P_{\mathrm{VM}} + P \cdot P_{\mathrm{MIX}} + 2 \cdot P \cdot P_{\mathrm{BB}} + 2 \cdot P \cdot P_{\mathrm{ADC}}. \quad (13)$$

Here, P_{VM} is the power consumed by a low-noise VM-amplifier and γ_{SP} is the analog combiner sparsity coefficient: $\gamma_{SP} = 1$ denotes a non-sparse $\boldsymbol{A}$, while $\gamma_{SP} = 0.75$ corresponds to 25% sparsity. The estimated power consumption of each hardware component and the total power consumption of task-specific and -agnostic MIMO receivers are summarized in Table I. The power scaling for various quantization levels of the VMs is based on [42] when using 8 bits for high-resolution VMs. For the ADC power estimation, we utilize Walden FoM [30], [41]. Our results show that the proposed power-saving techniques (25% sparsity, 4-bit VMs, 4-bit ADCs) provide more than 58% reduction in power compared to the task-agnostic MIMO architectures using high-resolution ADCs, high-power LNAs, and high-resolution VMs. These notable power gains add to the improved MSE performance shown in Fig. 2 and the spatial interferer rejection observed in Fig. 3.

V. CONCLUSIONS

In this work, we studied a power-efficient hybrid MIMO receiver design with embedded beamforming and low-resolution ADCs using task-specific quantization. We introduced a power-efficient analog and digital joint optimization framework, incorporating sparse analog combining and considering the finite resolution of the configurable analog pre-processing hardware. Furthermore, we demonstrated suppression of undesired spatial interferers to facilitate operation in congested spectrum environments. Supported by our numerical simulation results, the proposed hybrid MIMO receiver notably outperforms the task-agnostic MIMO receivers by achieving optimal MSE performance at lower power and lower quantization rate.

REFERENCES

[1] V. Wong, R. Schober, D. Ng, and L. Wang, *Key Technologies for 5G Wireless Systems*. Cambridge University Press, 2017.

[2] R. W. Heath Jr. and A. Lozano, *Foundations of MIMO Communication*. Cambridge University Press, 2018.

[3] M. Agiwal, A. Roy, and N. Saxena, "Next generation 5G wireless networks: A comprehensive survey," *IEEE Commun. Surveys Tuts.*, vol. 18, no. 3, pp. 1617–1655, 2016.

[4] N. Shlezinger and Y. C. Eldar, "On the spectral efficiency of non-cooperative uplink massive MIMO systems," *IEEE Trans. Commun.*, vol. 67, no. 3, pp. 1956–1971, 2018.

[5] H. Q. Ngo, E. G. Larsson, and T. L. Marzetta, "Energy and spectral efficiency of very large multiuser mimo systems," *IEEE Trans. Commun.*, vol. 61, no. 4, pp. 1436–1449, 2013.

[6] D. Gesbert, M. Shafi, D. shan Shiu, P. Smith, and A. Naguib, "From theory to practice: an overview of mimo space-time coded wireless systems," *IEEE J. Sel. Areas Commun.*, vol. 21, no. 3, pp. 281–302, 2003.

[7] F. Rusek, D. Persson, B. K. Lau, E. G. Larsson, T. L. Marzetta, O. Edfors, and F. Tufvesson, "Scaling up mimo: Opportunities and challenges with very large arrays," *IEEE Signal Process. Mag.*, vol. 30, no. 1, pp. 40–60, 2013.

[8] N. Shlezinger, Y. C. Eldar, and M. R. Rodrigues, "Asymptotic task-based quantization with application to massive MIMO," *IEEE Trans. Signal Process.*, vol. 67, no. 15, pp. 3995–4012, 2019.

[9] Y. C. Eldar, *Sampling Theory: Beyond Bandlimited Systems*. Cambridge University Press, 2015.

[10] R. Walden, "Analog-to-digital converter survey and analysis," *IEEE J. Sel. Areas Commun.*, vol. 17, no. 4, pp. 539–550, 1999.

[11] R. Méndez-Rial, C. Rusu, N. González-Prelcic, A. Alkhateeb, and R. W. Heath, "Hybrid MIMO architectures for millimeter wave communications: Phase shifters or switches?" *IEEE access*, vol. 4, pp. 247–267, 2016.

[12] S. S. Ioushua and Y. C. Eldar, "A family of hybrid analog-digital beamforming methods for massive MIMO systems," *IEEE Trans. Signal Process.*, vol. 67, no. 12, pp. 3243–3257, 2019.

[13] C. Huang, S. Hu, G. C. Alexandropoulos, A. Zappone, C. Yuen, R. Zhang, M. Di Renzo, and M. Debbah, "Holographic MIMO surfaces for 6G wireless networks: Opportunities, challenges, and trends," *IEEE Wireless Commun.*, vol. 27, no. 5, pp. 118–125, 2020.

[14] M. C. M. Soer, E. A. M. Klumperink, B. Nauta, and F. E. van Vliet, "Spatial interferer rejection in a four-element beamforming receiver front-end with a switched-capacitor vector modulator," *IEEE J. Solid-State Circuits*, vol. 46, no. 12, pp. 2933–2942, 2011.

[15] M. C. M. Soer, E. A. M. Klumperink, D.-J. van den Broek, B. Nauta, and F. E. van Vliet, "Beamformer with constant-gm vector modulators and its spatial intermodulation distortion," *IEEE J. Solid-State Circuits*, vol. 52, no. 3, pp. 735–746, 2017.

[16] H. Krishnaswamy and L. Zhang, "Analog and RF interference mitigation for integrated MIMO receiver arrays," *Proc. IEEE*, vol. 104, no. 3, pp. 561–575, 2016.

[17] S. Golabighezelahmad, E. A. Klumperink, and B. Nauta, "A 0.7-5.7 GHz reconfigurable MIMO receiver architecture for analog spatial notch filtering using orthogonal beamforming," *IEEE J. Solid-State Circuits*, 2020.

[18] J. Mo, A. Alkhateeb, S. Abu-Surra, and R. W. Heath, "Hybrid architectures with few-bit ADC receivers: Achievable rates and energy-rate tradeoffs," *IEEE Trans. Wireless Commun.*, vol. 16, no. 4, pp. 2274–2287, 2017.

[19] K. Roth, H. Pirzadeh, A. L. Swindlehurst, and J. A. Nossek, "A comparison of hybrid beamforming and digital beamforming with low-resolution ADCs for multiple users and imperfect CSI," *IEEE J. Sel. Topics Signal Process.*, vol. 12, no. 3, pp. 484–498, 2018.

[20] J. Choi, J. Sung, B. L. Evans, and A. Gatherer, "Antenna selection for large-scale MIMO systems with low-resolution ADCs," in *2018 IEEE International Conference on Acoustics, Speech and Signal Processing (ICASSP)*, 2018, pp. 3594–3598.

[21] Y. Li, C. Tao, G. Seco-Granados, A. Mezghani, A. L. Swindlehurst, and L. Liu, "Channel estimation and performance analysis of one-bit massive MIMO systems," *IEEE Trans. Signal Process.*, vol. 65, no. 15, pp. 4075–4089, 2017.

[22] N. Shlezinger, Y. C. Eldar, and M. R. Rodrigues, "Hardware-limited task-based quantization," *IEEE Trans. Signal Process.*, vol. 67, no. 20, pp. 5223–5238, 2019.

[23] P. Neuhaus, N. Shlezinger, M. Dörpinghaus, Y. C. Eldar, and G. Fettweis, "Task-based analog-to-digital converters," *IEEE Trans. Signal Process.*, vol. 69, pp. 5403–5418, 2021.

[24] N. Shlezinger and Y. C. Eldar, "Deep task-based quantization," *Entropy*, vol. 23, no. 1, p. 104, 2021.

[25] S. Salamatian, N. Shlezinger, Y. C. Eldar, and M. Médard, "Task-based quantization for recovering quadratic functions using principal inertia components," in *2019 IEEE International Symposium on Information Theory (ISIT)*, 2019, pp. 390–394.

[26] H. Wang, N. Shlezinger, Y. C. Eldar, S. Jin, M. F. Imani, I. Yoo, and D. R. Smith, "Dynamic metasurface antennas for MIMO-OFDM receivers with bit-limited ADCs," *IEEE Trans. Commun.*, vol. 69, no. 4, pp. 2643–2659, 2021.

[27] N. Shlezinger, R. J. G. van Sloun, I. A. M. Huijben, G. Tsintsadze, and Y. C. Eldar, "Learning task-based analog-to-digital conversion for MIMO receivers," in *ICASSP 2020 - 2020 IEEE International Conference on Acoustics, Speech and Signal Processing (ICASSP)*, 2020, pp. 9125–9129.

[28] F. Xi, N. Shlezinger, and Y. C. Eldar, "BiLiMO: Bit-limited MIMO radar via task-based quantization," *IEEE Trans. Signal Process.*, vol. 69, pp. 6267–6282, 2021.

[29] F. Ellinger, U. Mayer, M. Wickert, N. Joram, J. Wagner, R. Eickhoff, I. Santamaria, C. Scheytt, and R. Kraemer, "Integrated adjustable phase shifters," *IEEE Microwave Magazine*, vol. 11, no. 6, pp. 97–108, 2010.

[30] P. Skrimponis, S. Dutta, M. Mezzavilla, S. Rangan, S. H. Mirfarshbafan, C. Studer, J. Buckwalter, and M. Rodwell, "Power consumption analysis for mobile mmwave and sub-thz receivers," in *2020 2nd 6G Wireless Summit (6G SUMMIT)*, 2020, pp. 1–5.

[31] S. P. Boyd and L. Vandenberghe, *Convex optimization*. Cambridge University Press, 2004.

[32] S. Foucart and H. Rauhut, *A mathematical introduction to compressive sensing*. Springer, 2013.

[33] N. Shlezinger, J. Whang, Y. C. Eldar, and A. G. Dimakis, "Model-based deep learning," *arXiv preprint arXiv:2012.08405*, 2020.

[34] T. Chen, X. Chen, W. Chen, H. Heaton, J. Liu, Z. Wang, and W. Yin, "Learning to optimize: A primer and a benchmark," *arXiv preprint arXiv:2103.12828*, 2021.

[35] V. Monga, Y. Li, and Y. C. Eldar, "Algorithm unrolling: Interpretable, efficient deep learning for signal and image processing," *IEEE Signal Process. Mag.*, vol. 38, no. 2, pp. 18–44, 2021.

[36] S. Khobahi, N. Shlezinger, M. Soltanalian, and Y. C. Eldar, "LoRD-Net: Unfolded deep detection network with low-resolution receivers," *IEEE Trans. Signal Process.*, vol. 69, pp. 5651–5664, 2021.

[37] N. Joram, U. Mayer, R. Eickhoff, and F. Ellinger, "Fully integrated active cmos vector modulator for 802.11a compliant diversity transceivers," in *2009 IEEE International Conference on Microwaves, Communications, Antennas and Electronics Systems*, 2009, pp. 1–4.

[38] A. Amer, E. Hegazi, and H. F. Ragaie, "A 90-nm wideband merged cmos lna and mixer exploiting noise cancellation," *IEEE J. Solid-State Circuits*, vol. 42, no. 2, pp. 323–328, 2007.

[39] K. Kibaroglu and G. M. Rebeiz, "A 0.05–6 ghz voltage-mode harmonic rejection mixer with up to 30 dbm in-band iip3 and 35 dbc hrr in 32 nm soi cmos," in *2017 IEEE Radio Frequency Integrated Circuits Symposium (RFIC)*, 2017, pp. 304–307.

[40] C.-C. Ho and T.-C. Lee, "A 10-bit 200-ms/s reconfigurable pipelined a/d converter," in *Proceedings of Technical Program of 2012 VLSI Design, Automation and Test*, 2012, pp. 1–4.

[41] H.-S. Lee and C. G. Sodini, "Analog-to-digital converters: Digitizing the analog world," *Proc. IEEE*, vol. 96, no. 2, pp. 323–334, 2008.

[42] H. J. Qian, B. Zhang, and X. Luo, "High-resolution wideband phase shifter with current limited vector-sum," *IEEE Trans. Circuits Syst. I*, vol. 66, no. 2, pp. 820–833, 2019.

[43] B. Ginsburg and A. Chandrakasan, "A 500ms/s 5b adc in 65nm cmos," in *2006 Symposium on VLSI Circuits, 2006. Digest of Technical Papers.*, 2006, pp. 140–141.